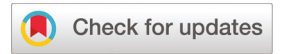
Nanoscale



PAPER

View Article Online
View Journal | View Issue



Cite this: Nanoscale, 2022, 14, 13771

Machine learning guided microwave-assisted quantum dot synthesis and an indication of residual H₂O₂ in human teeth†

Quan Xu, (1) ** Yaoyao Tang, ** Peide Zhu, ** Weiye Zhang, ** Yuqi Zhang, ** Oliver Sanchez Solis, ** Travis Shihao Hu** and Juncheng Wang***

The current preparation methods of carbon quantum dots (CDs) involve many reaction parameters, which leads to many possibilities in the synthesis processes and high uncertainty of the resultant production performance. Recently, machine learning (ML) methods have shown great potential in correlating the selected features in many applications, which can help understand the relevant structure–function relationships of CDs and discover better synthesis recipes as well. In this work, we employ the ML approach to guide the blue CD synthesis in microwave systems. After optimizing the synthesis parameters and conditions, the quantum yield (QY) increases to about 200% higher than the average value of the prepared samples without ML guidance. The obtained CDs are applied as fluorescent probes to monitor hydrogen peroxide (H_2O_2) in human teeth. The CD probe exhibits a linear relationship with the concentration of H_2O_2 ranging from 0 to 1.1 M with a lower detection limit of 0.12 M, which can effectively detect the residual H_2O_2 after bleaching teeth. This work shows that the adopted ML methods have considerable advantages in guiding the synthesis of high-quality CDs, which could accelerate the development of other novel functional materials in energy, biomedical, and environmental remediation applications.

Received 7th July 2022, Accepted 18th August 2022 DOI: 10.1039/d2nr03718a

rsc.li/nanoscale

Introduction

Hydrogen peroxide (H_2O_2) is an essential oxidizing, bleaching, and sterilizing agent in biochemical and chemical industries.¹ A high concentration of H_2O_2 may lead to serious health problems associated with asthma, cardiovascular disease, and cancer.² The rapid and precise determination of H_2O_2 is one of the crucial tasks in numerous fields. Several methods have been reported^{3,4} such as liquid chromatography,⁵ electrochemistry,⁶ electrochemiluminescence,⁷ colorimetric,⁸ and fluorescence methods,⁹ and so on. The fluorescence method based on carbon quantum dots (CDs) is popular because of its simplicity, high sensitivity, and rapid response.^{10,11} As a new class of fluorescent nanomaterials,¹² CDs have excellent optical properties,¹² low toxicity,¹³ and environmental friendli-

In the recent few years, with a rapid increase of computational power, and advanced hardware and software platforms, machine learning (ML) as the most important branch of artificial intelligence has entered the center stage of the scientific community.^{30,31} It has emerged with big data and high-performance computing to create new opportunities for

ness,14 which make them suitable for various applications in biosensors, 15,16 ion probes, 17-19 and cell imaging, 20-22 Due to their excellent physical and chemical properties and widespread application, many synthesis methods have been investigated. Compared with other strategies for synthesizing highquality CDs involving high cost and complexity, the microwave-assisted method is simple and quick,23 where the precursor is heated by the dielectric loss of the electromagnetic field. 24,25 Microwaves have been widely used in many processes of materials preparation²⁶ and chemical synthesis,²⁷ because of their excellent penetrating capabilities, 28 which allow the heating of samples/components quickly and uniformly.²⁹ Thus, this method offers a short synthesis time leading to an accelerated cycle of new material discovery.26 However, the optimization of the CD synthesis conditions needs a tedious trial-and-error process, which is unable to keep up with the pace of new materials development, calling for more efficient and effective strategies.

^aState Key Laboratory of Heavy Oil Processing, China University of Petroleum (Beijing), Beijing 102249, China. E-mail: xuquan@cup.edu.cn

^bDepartment of Mechanical Engineering, California State University, Los Angeles, California90032, USA

^cInstitute of Stomatology, First Medical Center, Chinese PLA General Hospital, Beijing 100853, China. E-mail: wbhwjc527@126.com

[†]Electronic supplementary information (ESI) available. See DOI: https://doi.org/ 10.1039/d2nr03718a

Paper Nanoscale

various applications in information science, 32,33 material synthesis, 34,35 material property prediction, 36 and the discovery of new compounds.³⁷ ML exhibited distinguished capability to accelerate the discovery of new materials by learning existing data and building data-driven models. 38-42 For example, Han et al.43 used ML to guide the synthesis of CDs in a hydrothermal system, improving the quantum yield by up to 39.9%. CDs prepared by machine learning-driven synthesis, which exhibits similar morphology and excellent performance, could be used as ultra-sensitive fluorescent probes for monitoring Fe³⁺ ions. Tang et al. 44 applied regression and classification algorithms by synthesizing CDs and growing chemical vapor deposited (CVD) MoS2, respectively. The yield of CDs and the growing conditions of MoS2 were highly precisely and accurately predicted. Wang et al.45 through the XGBoost model achieved CD-based white photoluminescence (PL) emission with adjustable correlated color temperature (CCT) from 3093 to 11 018 K. It is, therefore, appealing to introduce ML into CD synthesis to accelerate experimental trials, reduce energy consumption and get a desirable result, which is promising and potential.

In this study, ML is used to guide CD synthesis with enhanced yield by using the microwave method. An ML model is built on data obtained from experimental records and trained iteratively. Then, the model gives the best synthesis parameters and the QY is up to 15.7% through experimental verification. Besides, the correlation of the preparation parameters is analyzed by Pearson's correlation coefficient and grey relational analysis to obtain the inherent laws of these data. Furthermore, the photoluminescence of ML-guided CDs could be quenched by H_2O_2 , so they can be used as fluorescent probes for monitoring H_2O_2 in the concentration range of 0–1.1 M and with a detection limitation of 0.12 M. Then it can effectively test the trace of H_2O_2 after bleaching teeth. Overall,

the strategy of using ML to guide the microwave-assisted synthesis of CDs is of practical importance and it helps to break new ground in synthesizing other advanced functional micro-/nanomaterials in the future.

Experimental method

Source of data and data processing

A schematic diagram of ML guided microwave-assisted CDs is shown in Fig. 1 and the detailed synthesis of CDs is provided in the experimental section. The experimental records include the mass of the precursor (M_P) , the volume of EDA $(V_{\rm EDA})$, the volume of deionized water $(V_{\rm W})$, microwave intensity $(I_{\rm M})$, microwave time $(T_{\rm M})$, and the quantum yield (QY). QY is the output feature and others are considered input features. The internal data association between the input features and the output features aims to improve the QY properties through machine learning algorithms. 190 experimental records are retrieved from our sets of data obtained from experimental preparation records and QY (%) ranging from 0 to 100, respectively. The distribution histogram of microwave-assisted synthesis of CD data for each of the parameters is shown in Fig. S1.† More details about these data are summarized in ESI Table S1.† The data set is enough to construct models as shown in Fig. S2.†

Pearson's correlation coefficient (PCC) among the 5 parameters is calculated and the corresponding heat map is presented in Fig. 2(a), which indicates that there is no strong correlation among these parameters and is satisfied with the independence requirement. Therefore, these 5 parameters could be used as the input features of the ML models. Moreover, the grey correlation analysis is performed to analyze the importance of these five features on QY as shown in

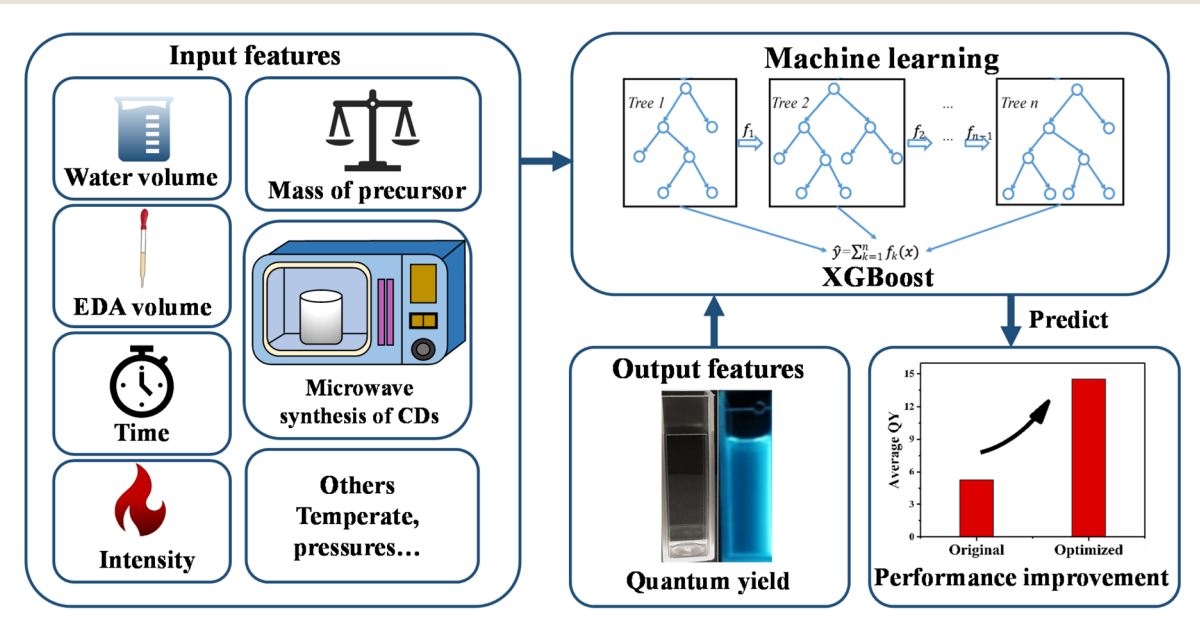


Fig. 1 Framework for the guided synthesis of CDs by the microwave method based on ML

Nanoscale Paper

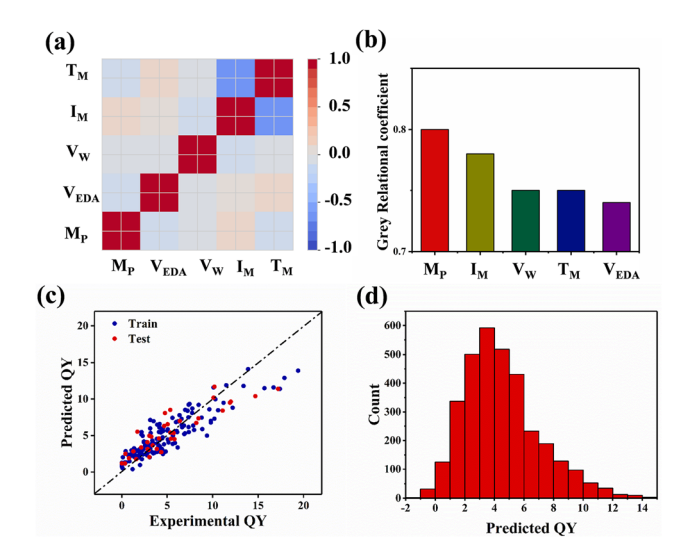


Fig. 2 (a) The heat map of Pearson's correlation coefficient among the selected features of the microwave. (b) The histogram of the grey relational coefficient of the selected feature to QY relationships. (c) Comparison between the experimental and predicted values for the train data set (blue dot) and test data set (red dot). (d) The histogram of the predicted QY distribution.

Fig. 2(b). This indicates that the mass of the precursor and the microwave intensity affect the QY the most.

According to the law of mass action, the mass of the precursor determines its concentration in the solution and the term controls the nucleation rate of CDs, which affects the kinetics of the crystal growth. Besides, microwave intensity affects the heating rate and the temperature of the system. This parameter also affects the kinetics of CD growth as described by the Arrhenius equation. Therefore, these two features are expected to influence the synthesis of CDs synergistically in terms of the QY.

Model selection and optimization

The data set before the training model is normalized by the maximum and minimum values to eliminate the multiscale nature, which is all converted to a range between 0 and 1. To find the appropriate model for this problem, we test the performance of the decision tree (DT), multilayer perceptron (MLP), random forest (RF), and XGBoost (XGB) simultaneously under the same train data. These models are optimized by five-fold cross-validation and evaluated through performance metrics including mean squared error (MSE), mean absolute

error (MAE), coefficient of determination (R2), and PCC. The performance metrics of the four models are shown in box plots in Fig. S3.† Considering the generalization ability and fitting outcome, XGBoost is selected as the best ML model. Fig. 2(c) shows that the predicted value and experimental value have a linear relationship with all data, which demonstrates the excellent performance of XGB.

Prediction

The constructed XGB model is trained with 190 experimental records, and it is employed to predict the QY. Through input ranges of each feature generating 3300 synthesis combinations, all these data are the predicted QYs by the XGB model. Fig. 2(d) shows the distribution histogram of all the predicted data, and it can be seen that the overall predicted yield is normally distributed, which indicates the selection of data points is reasonable. Among these predicted QY results, five synthesis combinations with the highest predicted QY were chosen and experiments are performed to verify the yield. A high QY of 15.7% was achieved as shown in Table 1, which is about 200% higher than the average value of the overall historical QY, indicating the feasibility and effectiveness of MLguided microwave-assisted CD synthesis. To better understand the internal raw data, the predicted result is shown using a matrix map with the most important feature (Fig. S4†). The redder the area, the higher the QY with a combination of the corresponding conditions. With an increase in the mass of the precursor and microwave intensity, the QY improves obviously, which is consistent with the previous grey correlation analysis.

Results and discussion

Characterization of CDs

Based on the strategy of ML, the experimental synthesis has the highest QY of CDs. The transmission electron microscope (TEM) was used to investigate the diameter of the optimized CDs. As shown in Fig. 3(a), the CDs are well-dispersed in water solution and the distribution diagram (Fig. 3(b)) implies that the particle size ranges from 3.25 to 6.25 nm, with an average diameter of 4.8 nm. The high-resolution TEM (HRTEM) image (the inset of Fig. 3(a)) shows a clear crystal lattice with a lattice fringe distance of 0.21 nm, which corresponds to the (100) lattice plane of graphite carbon.46 The X-ray diffractometer (XRD) pattern of the CDs (Fig. 3(c)) displays a broad peak centered at ~18°, which may be related to the small size of the

Table 1 Combinations with the highest probability

No.	Mass of precursor A (g)	EDA volume (ml)	Water volume (ml)	Microwave intensity (%)	Microwave time (min)	QY (%)	Experimental QY (%)
1	1.5	0.55	10	100	3	14.23	13.4
2	1.5	0.55	10	58	3	14.14	13.9
3	1.5	0.55	20	100	3	14.13	12.5
4	1.5	0.55	15	100	3	13.94	13.6
5	1.5	0.60	10	100	3	13.92	15.7

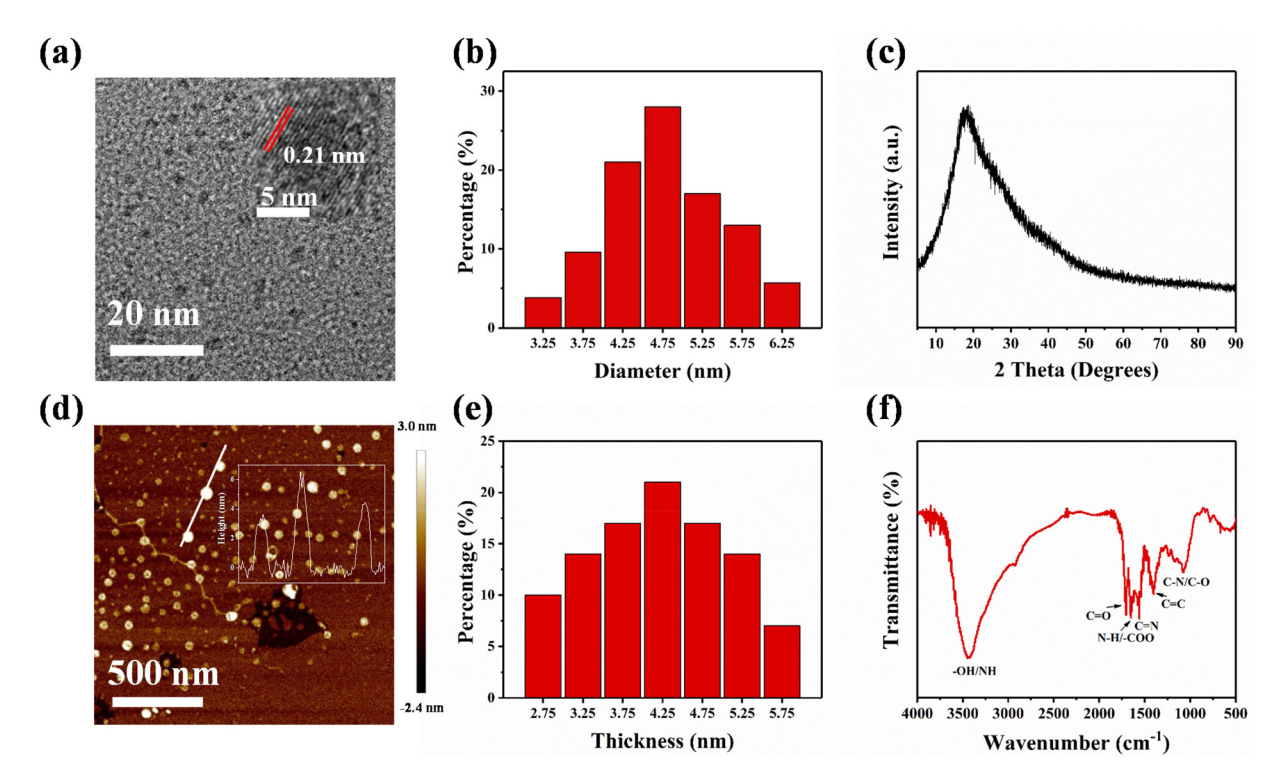


Fig. 3 Characterization of the ML-assisted synthesis of CDs. (a) TEM image of CDs (insert: HRTEM image). (b) The diameter distribution of CDs. (c) The XRD pattern of CDs. (d) AFM image of CDs (inset: height profile of the corresponding line in the AFM image). (e) The thickness distribution of CDs. (f) FT-IR spectrum of CDs.

CDs. 47,48 The topographic morphology of the CDs was further measured by atomic force microscopy (AFM). In Fig. 3(d) and (e), the image of CDs provides an average thickness of 4.25 nm. These graphs show that the CDs produced by the MLassisted method have a uniform size and also have an elliptical structure, which agrees well with the definition of CDs. We also studied the chemical structure of the CDs. As shown in Fig. 3(f), there are six obvious FTIR peaks at 3445, 1725, 1650, 1642, 1524, and 2239 cm⁻¹. The peak at 3445 cm⁻¹ is attributed to the -OH/-NH group, which gives them high solubility in water.46 The -NH and C=N stretching vibrations (at about 3445 and 1642 cm⁻¹) indicate that there are a huge number of -NH groups on the surface of CDs. 49,50 The peak at 1725 cm⁻¹ is attributed to the C=O stretching vibration due to abundant hydroxyl groups in the precursor, 43 and the peak at 1650 cm⁻¹ is a direct result of N-H and -COO stretching vibrations. 17

C=C and C=N stretching vibrations are observed at 1524 cm⁻¹ and 1642 cm⁻¹, respectively. The peak at 1139 cm⁻¹ is assigned to the C-N and C-O bending vibrations.⁵¹ UV-vis absorption spectroscopy, Fourier transform infrared (FT-IR) spectroscopy and X-ray photoelectron spectroscopy (XPS) were used to verify the structure and chemical bonds of the CDs. The UV-vis absorption spectrum of CDs (Fig. 4(a)) shows a typical absorption peak at 237 nm corresponding to the π - π * transition.⁵² We also studied the optical properties of the CDs. Fig. 4(b) shows the illumination characteristics with excitation wavelengths from 290 nm to 400 nm. The peak positions of varied excitation wavelengths are almost identical and the peak intensity decreases, which indicates the inexistence of excitation wavelength-dependent emission properties of the CDs. 53 The optimal emission occurs at a wavelength of 480 nm when excited by a 320 nm light source. To investigate the CD solution stability, the fluorescence intensity was measured every ten minutes as shown in Fig. S5(a).† The PL intensity of CDs remained unchanged within 60 min, and above 99% during the stability test.

Besides, we performed XPS analysis. The full spectrum of XPS (Fig. 4(c)) shows three typical peaks at 285, 400, and 531 eV, corresponding to C 1s, N 1s, and O 1s, respectively. 51,54 In Table S3,† the proportions of the three elements including C, N, and O are 66.27%, 23.32%, and 10.41%, respectively. As shown in Fig. 4(d), the high-resolution C 1s spectra of CDs can be deconvoluted into three peaks at 284.6 eV, 286.1 eV, and 288.2 eV, corresponding to sp² carbon C=C, -COOH, and C-N/C=N.51,55,56 The nitrogen atoms were identified in highresolution N1s spectra in Fig. 4(e). Three peaks at 398.4 eV, 399.6 eV, and 400.8 eV correspond to pyridine N, pyrrole N, and graphite N, respectively.⁵¹ Nitrogen exists in various forms and forms a π bond conjugated O with C, suggesting that the nitrogen is successfully doped into the CD structure.51 The O 1s XPS spectra in Fig. 4(f) are fitted by four peaks, including carboxyl group (-COOH) and C=O, confirmed by C1s. Besides, the high-resolution O 1s peaks at 533 eV and 530.6 eV correspond to C-O and O-H, indicating that the CDs could easily

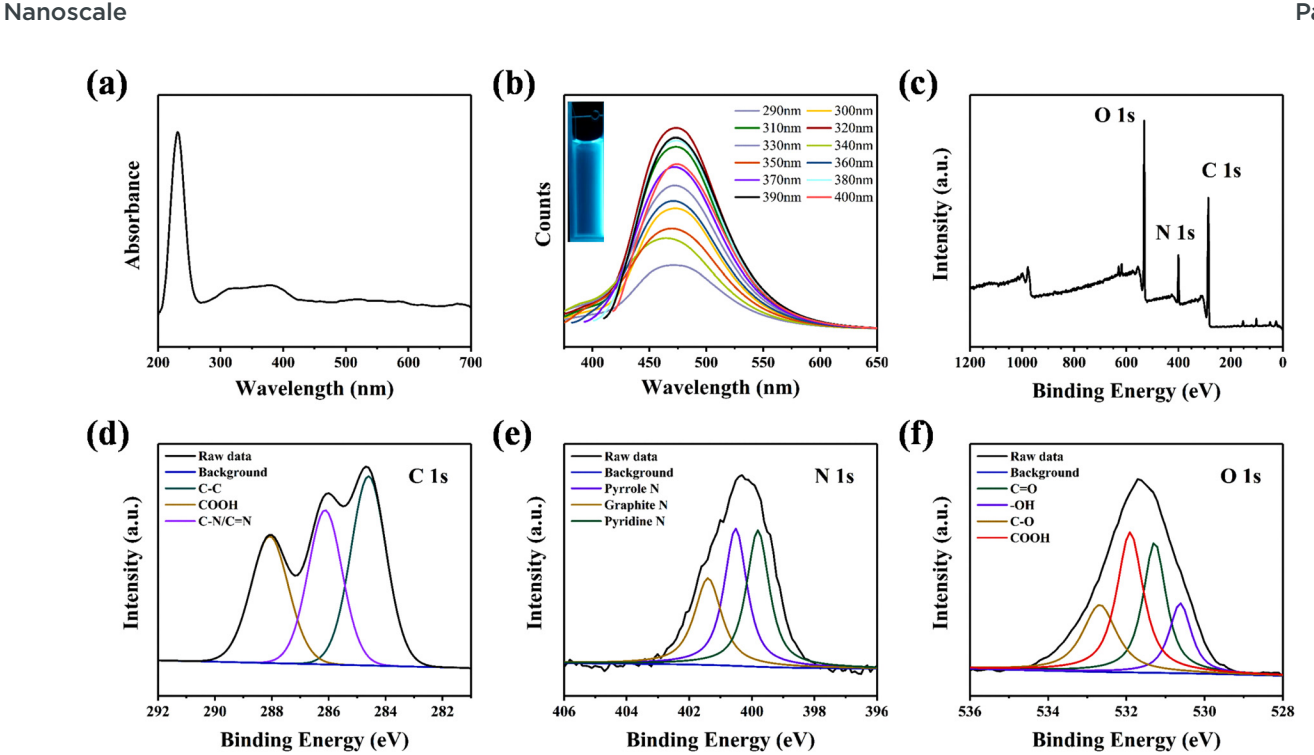


Fig. 4 (a) The UV-vis absorption wavelength of the CDs. (b) Fluorescence emission spectra of the prepared CDs at different excitation wavelengths. (c)XPS survey spectrum of CDs. XPS (d) C1s, (e) N1s, and (f) O1s spectra of CDs, respectively.

dissolve in water.⁵⁵ The above FT-IR and XPS analyses show that the abundant hydrophilic functional groups on the surface of CDs not only provide interaction sites for specific ions or compounds but also improve the dispersion of CDs.

Detection of H₂O₂

 $\rm H_2O_2$ acts as a strong oxidant by consuming antioxidant substances in the body, causing low antioxidant capacity and reducing resistance, which further causes various diseases. Besides, $\rm H_2O_2$ has certain harmful effects on the human body, which causes DNA damage and mutation of the human genetic material. Therefore, the determination of $\rm H_2O_2$ has an important role in the biological health field. The prepared CDs as fluorescent probes are used to detect the concentration of $\rm H_2O_2$ due to the rapid and sensitive response to $\rm H_2O_2$. Fig. 5(a) shows that the fluorescence intensity decreases with a gradual increase of the concentration of $\rm H_2O_2$. The fluorescence intensity has a linear relationship with the concentration of $\rm H_2O_2$ ranging from 0 to 1.1 M, with a correlation coefficient of 0.983 (Fig. 5(b)).

The detection limit is 0.12 mM according to 3 σ/s (where σ is the standard deviation of the blank measurement and s is the slope of the calibration graph). To understand the fluorescence quenching process of the CDs, the lifetime and absorption are studied. As shown in Fig. 5(c), the time-dependent single-photon counting spectra of the CDs are reduced from 8.24 ns to 7.99 ns due to the quenched CD solution. Besides, the UV-vis absorption spectrum is recorded before and after quenching by adding H_2O_2 to an aqueous solution of

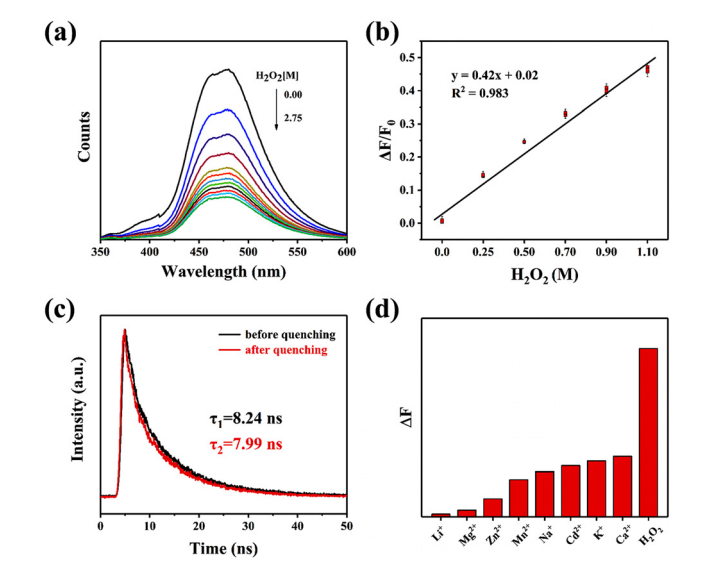


Fig. 5 (a) The effect of H_2O_2 quenching on the PL intensity of CDs, and (b) the change in the $\Delta F/F_0$ intensity of CD solution *versus* the concentration of H_2O_2 at 480 nm at an excitation wavelength of 320 nm. (c) The comparison of the illumination lifetime before and after H_2O_2 quenching. (d) The selective sensitivity of CDs.

CDs. The change in the absorption spectrum can be observed in Fig. S5(b).† Both of the above phenomena indicate a dynamic quenching mechanism. 58 Thus, it is reasonable to speculate charge transfer between $\rm H_2O_2$ and CDs leading to fluorescence quenching. To further verify the selectivity probe

Paper

to H₂O₂, we tested the CDs in various ion solutions with a concentration of 200 µM, including Li⁺, Mg²⁺, Zn²⁺, Mn²⁺, Na⁺, Cd^{2+} , K^+ , and Ca^{2+} , as shown in Fig. 5(d). We use $\Delta F = F_0 - F_1$ as an indicator, where F_0 is the fluorescence intensity at an excitation wavelength of 320 nm before the ions were introduced into the CDs, and F_1 is that after ions were added into the mixture. It is demonstrated that the CDs are most sensitive toward H₂O₂ above all the ions.

The indication of the H₂O₂ residue on teeth after bleaching

H₂O₂ is recognized as the primary potent bleaching agent by oxidizing organic colorants in dentin, 59-61 which would remain on the surface of the teeth and erode the hard and soft tissue in the oral cavity.⁶² In addition, H₂O₂ can easily enter tissues and cells in the body after oral intake, which can enter the free radical reaction chain, causing apoptosis and cancer, accelerating human aging and even inducing cardiovascular disease. So, we should indicate the residual on the surface of teeth and the method is shown in Fig. 6(a). The H₂O₂ on the surface of bleached teeth can quench the CDs, whose fluorescence intensity represents the H₂O₂ residue. Therefore, we collect four teeth and polished one side of the dentin flatly, and the surface of the tooth has yellow pigment deposition.

Two of the teeth are put into deionized water and one of them is the control group, and others are soaked in hydrogen peroxide solutions with volume fractions of 5% and 10%, respectively. After placing for 24 h in a dark and light-protected environment, the surface of the teeth is observed as shown in Fig. S6 and S7.† The tooth put into deionized water has no obvious change and others put into H2O2 lighten and change clearly. Moreover, the higher the concentration of H₂O₂, the more obvious the surface color of the teeth changes.

To indicate the H₂O₂ residue on teeth, we add 10 μL of CD solution to the polished surface and the control group was added with the same amount of deionized water (Fig. S8†). As shown in Fig. 6(c-e), the fluorescence of the experimental group is decreased with an increase in H₂O₂. It demonstrates that the CDs can effectively indicate the H₂O₂ residue on teeth after bleaching, and fluorescence relative to the concentration of H2O2 before soaking. Furthermore, the CDs are tested in ionic and wide pH solutions of different concentrations.

As shown in Fig. 6(b), it can be seen that the NaCl solution does not interfere with the fluorescence of the CDs, indicating the stability of CDs in an ionic solution of high concentration. Fig. S9† shows that the photoluminescence of the CDs remained almost unchanged in different pH solutions ranging

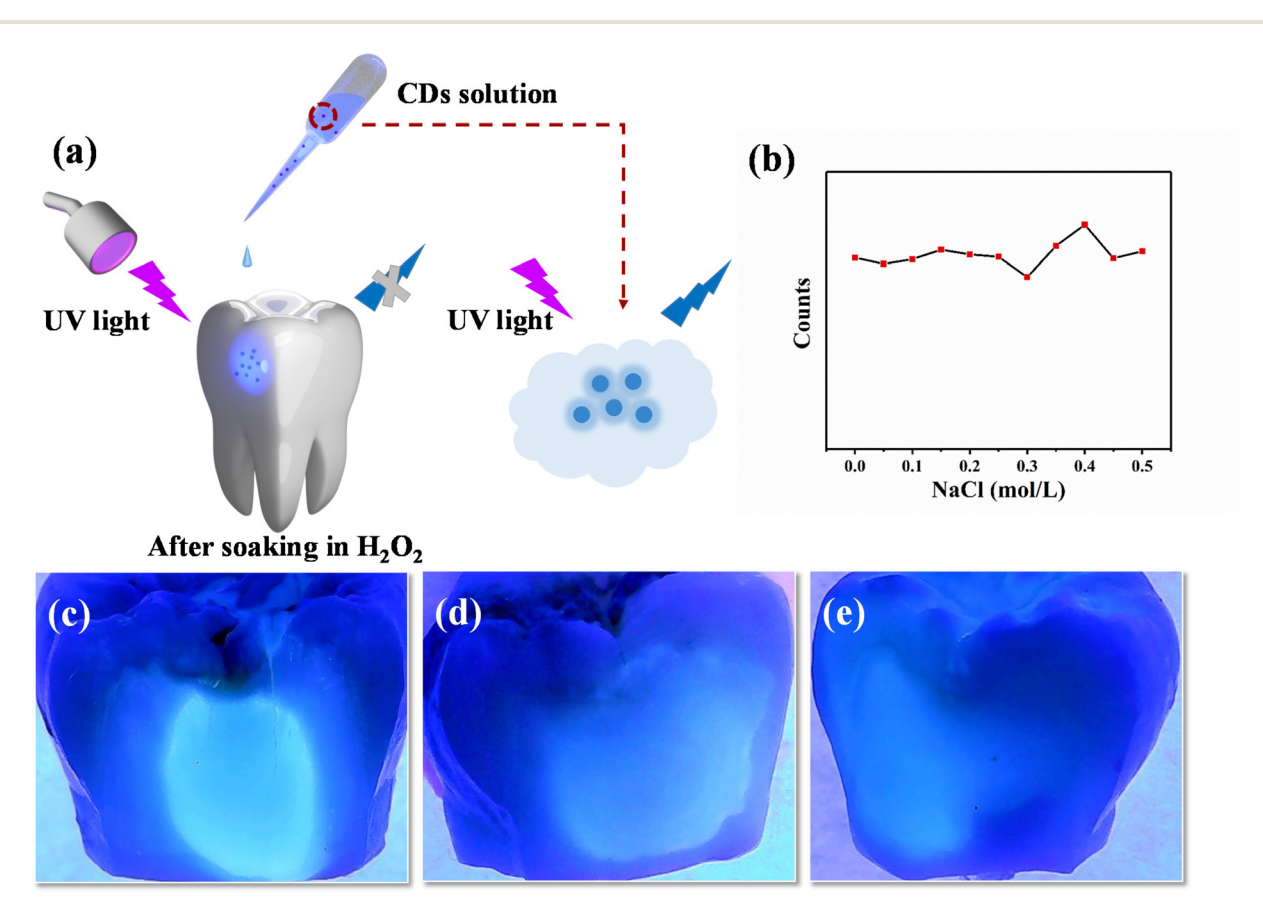


Fig. 6 (a) The schematic illustration for indicating the H₂O₂ residue by CDs on teeth after bleaching. (b) The stability of CDs vs. NaCl solution. The fluorescence of CDs on the teeth surface after adding CD solution under UV light. The teeth were soaked in deionized water (c), and in hydrogen peroxide solutions with volume fractions of 5% (d) and 10% (e), respectively.

Nanoscale Paper

from 1 to 12. So the wide range and stability of strong fluorescence make it versatile and applicable under more extreme tooth conditions.

Conclusion

In summary, the present work demonstrates the application of ML in the synthesis of inorganic functional nanomaterials through data processing, model selection, and model prediction. ML predicts the properties of CDs using the microwaveassisted method, which effectively improves the QY by up to 15.7%. It demonstrates that the ML can reveal some underlying relationships between data, helping to 'mine' the connection between features and results, and discover optimized synthesis conditions. The optimal CDs can be employed as sensing probes of high sensitivity and selectivity to detect H₂O₂. The probe has a wide detection range from 0 to 1.1 M, with a sensitivity limit of 0.12 M. Then the optimized CDs are applied to the teeth to indicate the residuals effectively. More importantly, our work demonstrates great potential for introducing ML into synthesizing materials and the data-driven model is effective in future development. We believe that this data-driven model can serve as a possible way to reduce experimental costs and accelerate material synthesis.

Conflicts of interest

There are no conflicts to declare.

Acknowledgements

Quan Xu acknowledges the support from the National Natural Science Foundation of China (No. 52211530034 and 51875577) and the Beijing National Science Foundation (No. 3222018), J. C. Wang acknowledges the support from the Military Health Care Project (22BJZ22), T. S. H. acknowledges the support from the U.S. National Science Foundation (Award No. 2004251 and 1523588).

References

- 1 S. K. Bhunia, S. Dolai, H. Sun and R. Jelinek, *Sens. Actuators*, *B*, 2018, 270, 223-230.
- 2 S. Parthasarathy, V. Nandhini and B. Jeyaprakash, *J. Colloid Interface Sci.*, 2016, **482**, 81–88.
- 3 M. R. Rojas, C. Leung, D. Whitley, Y. Zhu, R. G. Arnold and A. E. Sáez, *Ind. Eng. Chem. Res.*, 2011, **50**, 12479–12487.
- 4 Y. Wang, Z. Chen, Y. Liu and J. Li, *Nanoscale*, 2013, 5, 7349–7355.
- 5 S. M. Steinberg, *Environ. Monit. Assess.*, 2013, **185**, 3749–3757.
- 6 W. H. Antink, Y. Choi, K.-D. Seong and Y. Piao, *Sens. Actuators*, *B*, 2018, 255, 1995–2001.
- 7 S. Ge, J. Zhao, S. Wang, F. Lan, M. Yan and J. Yu, *Biosens. Bioelectron.*, 2018, **102**, 411–417.

- 8 H. Liu, Y. Ding, B. Yang, Z. Liu, Q. Liu and X. Zhang, Sens. Actuators, B, 2018, 271, 336–345.
- 9 T. Lin, Y. Qin, Y. Huang, R. Yang, L. Hou, F. Ye and S. Zhao, *Chem. Commun.*, 2018, 54, 1762–1765.
- 10 W. Teo, A. V. Caprariello, M. L. Morgan, A. Luchicchi, G. J. Schenk, J. T. Joseph, J. J. Geurts and P. K. Stys, *Proc. Natl. Acad. Sci. U. S. A.*, 2021, 118.
- 11 S. Mueller, J. Lüttig, L. Brenneis, D. Oron and T. Brixner, ACS Nano, 2021, 15, 4647–4657.
- 12 Y. Sun, B. Zhou and Y. Lin, *J. Am. Chem. Soc.*, 2006, **128**, 7756–7757.
- 13 N. Shi, K. Sun, Z. Zhang, J. Zhao, L. Geng and Y. Lei, *J. Ind. Eng. Chem.*, 2021, **101**, 372–378.
- 14 T.-Y. Wang, C.-Y. Chen, C.-M. Wang, Y. Z. Tan and W.-S. Liao, *ACS Sens.*, 2017, 2, 354–363.
- S. Zhu, Q. Meng, L. Wang, J. Zhang, Y. Song, H. Jin,
 K. Zhang, H. Sun, H. Wang and B. Yang, *Angew. Chem.*,
 2013, 125, 4045–4049.
- 16 K. Hola, Y. Zhang, Y. Wang, E. P. Giannelis, R. Zboril and A. L. Rogach, *Nano Today*, 2014, 9, 590–603.
- 17 Q. Xu, P. Pu, J. Zhao, C. Dong, C. Gao, Y. Chen, J. Chen, Y. Liu and H. Zhou, *J. Mater. Chem. A*, 2015, 3, 542–546.
- 18 Q. Xu, Y. Liu, C. Gao, J. Wei, H. Zhou, Y. Chen, C. Dong, T. S. Sreeprasad, N. Li and Z. Xia, *J. Mater. Chem. C*, 2015, 3, 9885–9893.
- 19 Q. Xu, M. Zhang, Y. Liu, W. Cai, W. Yang, Z. He, X. Sun, Y. Luo and F. Liu, New J. Chem., 2018, 42, 10400–10405.
- 20 H. Li, X. Yan, S. Qiao, G. Lu and X. Su, ACS Appl. Mater. Interfaces, 2018, 10, 7737-7744.
- 21 H. Ding, L.-W. Cheng, Y.-Y. Ma, J.-L. Kong and H.-M. Xiong, *New J. Chem.*, 2013, 37, 2515–2520.
- 22 A. R. Chowdhuri, S. Tripathy, C. Haldar, S. Roy and S. K. Sahu, *J. Mater. Chem. B*, 2015, 3, 9122–9131.
- 23 H. M. Ng, G. Lim and C. Leo, *Microchem. J.*, 2021, **165**, 106116.
- 24 T. V. de Medeiros, J. Manioudakis, F. Noun, J.-R. Macairan, F. Victoria and R. Naccache, *J. Mater. Chem. C*, 2019, 7, 7175–7195.
- 25 X. Wang, B. Wang, H. Wang, T. Zhang, H. Qi, Z. Wu, Y. Ma, H. Huang, M. Shao and Y. Liu, *Angew. Chem.*, 2021, 133, 12693–12698.
- 26 G. Yang and S.-J. Park, Materials, 2019, 12, 1177.
- 27 D. Bogdal, P. Penczek, J. Pielichowski and A. Prociak, Liquid chromatography/FTIR microspectroscopy/microwave assisted synthesis, 2003, pp. 194–263.
- 28 E. Grant and B. J. Halstead, Chem. Soc. Rev., 1998, 27, 213–224.
- 29 C. O. Kappe, Angew. Chem., Int. Ed., 2004, 43, 6250-6284.
- 30 X.-D. Zhang, in *A Matrix Algebra Approach to Artificial Intelligence*, Springer, 2020, pp. 223–440.
- 31 M. I. Jordan and T. M. Mitchell, Science, 2015, 349, 255-260.
- 32 W. Zong and G.-B. Huang, *Neurocomputing*, 2011, 74, 2541–2551.
- 33 R. Normand, W. Du, M. Briller, R. Gaujoux, E. Starosvetsky, A. Ziv-Kenet, G. Shalev-Malul, R. J. Tibshirani and S. S. Shen-Orr, *Nat. Methods*, 2018, 15, 1067–1073.

Paper Nanoscale

- 34 K. T. Butler, D. W. Davies, H. Cartwright, O. Isayev and A. Walsh, Nature, 2018, 559, 547-555.
- 35 F. Legrain, J. Carrete, A. van Roekeghem, G. K. Madsen and N. Mingo, J. Phys. Chem. B, 2018, 122, 625-632.
- 36 Y. Hayashi, Y. Nakano, Y. Marumo, S. Kumada, K. Okada and Y. Onuki, Int. J. Pharm., 2021, 121158, DOI: 10.1016/j. ijpharm.2021.121158.
- 37 A. Pulido, L. Chen, T. Kaczorowski, D. Holden, M. A. Little, S. Y. Chong, B. J. Slater, D. P. McMahon, B. Bonillo, C. J. Stackhouse, A. Stephenson, C. M. Kane, R. Clowes, T. Hasell, A. I. Cooper and G. M. Day, Nature, 2017, 543, 657-664.
- 38 N. C. Frey, J. Wang, G. I. Vega Bellido, B. Anasori, Y. Gogotsi and V. B. Shenoy, ACS Nano, 2019, 13, 3031-3041
- 39 E. Kim, K. Huang, A. Saunders, A. McCallum, G. Ceder and E. Olivetti, Chem. Mater., 2017, 29, 9436-9444.
- 40 E. Kim, K. Huang, A. Tomala, S. Matthews, E. Strubell, A. Saunders, A. McCallum and E. Olivetti, Sci. Data, 2017, **4**, 1-9.
- 41 Z. Li, Q. Xu, Q. Sun, Z. Hou and W. J. Yin, Adv. Funct. Mater., 2019, 29, 1807280.
- 42 H. Masood, C. Y. Toe, W. Y. Teoh, V. Sethu and R. Amal, ACS Catal., 2019, 9, 11774-11787.
- 43 Y. Han, B. Tang, L. Wang, H. Bao, Y. Lu, C. Guan, L. Zhang, M. Le, Z. Liu and M. Wu, ACS Nano, 2020, 14, 14761-
- 44 B. Tang, Y. Lu, J. Zhou, T. Chouhan, H. Wang, P. Golani, M. Xu, Q. Xu, C. Guan and Z. Liu, Mater. Today, 2020, 41, 72-80.
- 45 X. Wang, B. Wang, H. Wang, T. Zhang, H. Qi, Z. Wu, Y. Ma, H. Huang, M. Shao, Y. Liu, Y. Li and Z. Kang, Angew. Chem., Int. Ed., 2021, 60, 12585-12590.
- 46 P. Zhu, X. Zhao, X. Chen, S. Li, J. Ma, J. Li, M. Xu, L. Gan and Q. Xu, New J. Chem., 2021, 45, 10798-10801.

- 47 M. Lan, Y. Di, X. Zhu, T. W. Ng, J. Xia, W. Liu, X. Meng, P. Wang, C. S. Lee and W. Zhang, Chem. Commun., 2015, **51**, 15574-15577.
- 48 C. Liu, P. Zhang, X. Zhai, F. Tian, W. Li, J. Yang, Y. Liu, H. Wang, W. Wang and W. Liu, Biomaterials, 2012, 33, 3604-3613.
- 49 L. Wang, M. Li, W. Li, Y. Han, Y. Liu, Z. Li, B. Zhang and D. Pan, ACS Sustainable Chem. Eng., 2018, 6, 12668-12674.
- 50 L. Jiang, H. Ding, S. Lu, T. Geng, G. Xiao, B. Zou and H. Bi, Angew. Chem., 2020, 132, 10072-10077.
- 51 A. Kundu, B. Park, J. Oh, K. V. Sankar, C. Ray, W. S. Kim and S. C. Jun, Carbon, 2020, 156, 110-118.
- 52 Q. Li, Y. Li, S. Meng, J. Yang, Y. Qin, J. Tan and S. Qu, J. Mater. Chem. C, 2021, 9, 6796-6801.
- 53 Y. Zhang, Y. Hu, J. Lin, Y. Fan, Y. Li, Y. Lv and X. Liu, ACS Appl. Mater. Interfaces, 2016, 8, 25454-25460.
- 54 C. Wang and G. G. Wallace, Electrochim. Acta, 2015, 175, 87-95.
- 55 V. Saraswat, R. Kumari and M. Yadav, J. Phys. Chem. Solids, 2022, 160, 110341.
- 56 S. Chandra, D. Laha, A. Pramanik, A. Ray Chowdhuri, P. Karmakar and S. K. Sahu, Luminescence, 2016, 31, 81-87.
- 57 J. M. Bolivar, S. Schelch, M. Pfeiffer and B. Nidetzky, J. Mol. Catal. B: Enzym., 2016, 134, 302-309.
- 58 F. Zu, F. Yan, Z. Bai, J. Xu, Y. Wang, Y. Huang and X. Zhou, Microchim. Acta, 2017, 184, 1899-1914.
- 59 Y. Li, S. S. Lee, S. L. Cartwright and A. C. Wilson, Compendium of continuing education in dentistry (Jamesburg, NJ: 1995), 2003, vol. 24, pp. 357-360, 362, 364 passim; quiz 378.
- 60 Y. Li, Compendium of Continuing Education in dentistry (Jamesburg, NJ: 1995), Supplement, 2000, S4-S9; quiz S48.
- 61 M. Ward and H. Felix, Compendium of continuing education in dentistry (Jamesburg, NJ: 1995), 2012, vol. 33, pp. 286-291.
- 62 Y. Li, Dent. Clin., 2011, 55, 255-263.